ACS APPLIED MATERIALS & INTERFACES

Research Article

www.acsami.org

In Situ Synthesis of Self-Assembled Three-Dimensional Graphene–Magnetic Palladium Nanohybrids with Dual-Enzyme Activity through One-Pot Strategy and Its Application in Glucose Probe

Xuejing Zheng,[†,‡] Qian Zhu,[†,‡] Huiqing Song,[†,‡] Xinrui Zhao,[†,‡] Tao Yi,[▽] Hongli Chen,*[,†,‡,§] and Xingguo Chen[†,‡,§]

[†]National Key Laboratory of Applied Organic Chemistry, Lanzhou University, Lanzhou 730000, China

[‡]Department of Chemistry, Lanzhou University, Lanzhou 730000, China

[§]Key Laboratory of Nonferrous Metal Chemistry and Resources Utilization of Gansu Province, Lanzhou 730000, China

[▽]School of Chinese Medicine, Hong Kong Baptist University, Hong Kong, China

Supporting Information

ABSTRACT: The self-assembled three-dimensional graphene nanohybrids with *in situ*-formed Fe_3O_4 and Pd nanoparticles on it (3DRGO_Fe_3O_4-Pd) are first synthesized by the one-pot solvothermal method, which have intrinsic peroxidase-like and oxidase-like activity. The catalytic mechanism is analyzed by the electron spin resonance (ESR), fluorescence, and electrochemical methods. The mimic enzyme catalytic activity of 3DRGO_Fe_3O_4-Pd is much higher than those of monometallic loaded nanohybrids and their physical mixture, probably caused by synergistic effect between Pd and Fe_3O_4 nanoparticles. The 3DRGO_Fe_3O_4-Pd nanohybrids was reproducible, stable, and reusable. After 10 cycles, the catalytic activity was still higher than 90%, and the morphology and structure were basically unchanged. Based on its high peroxidase-like activity, especially the enhanced affinity toward H_2O_2, a new colorimetric detection method for reduced glutathione (GSH) and glucose has been designed using H_2O_2 as an intermediary, which provides a simple, sensitive, and selective way to detect urine glucose of diabetes with a wide linear range and low detection limit.

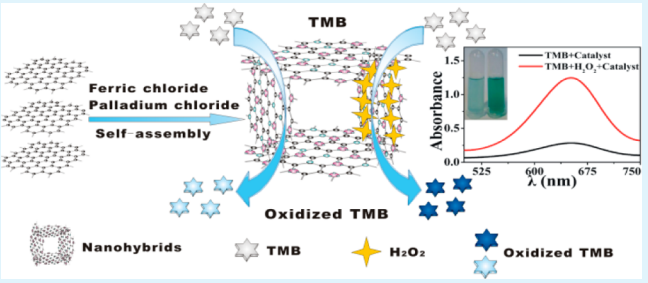

KEYWORDS: *one-pot, three-dimensional graphene nanohybrids, dual-enzyme activity, colorimetry, glucose*

INTRODUCTION

Two-dimensional (2D) graphene sheets possess the combination of remarkable electrical, optical, thermal, and mechanical properties.[1−3] Moreover, the abundant functional groups on the surfaces of graphene oxide sheets also provide many favorable sites for anchoring the functional nanocomponents.[4] Hence, 2D graphene-based materials have shown great potential for many applications. However, the strong planar stacking of 2D graphene sheets by forming irreversible agglomerates can lead to a drastic loss of active sites.[5,6] Consequently, three-dimensional (3D) porous graphene-based nanohybrids, especially metal nanoparticles anchored 3D graphene structures, are highly desirable, not only for stability of graphene sheets but also for immobilization of other metal particles. Meanwhile, 3D graphene nanostructure can facilitate the mass transfer and maximize the accessibility to the catalyst surfaces.[7,8] Because of the high surface-to-volume ratio of 3D graphene and reduced agglomeration between nanomaterials,[9] its applicability was greatly enhanced in various aspects, such as transparent conductive thin films,[10,11] anodes for lithium ion batteries,[12] supercapacitors,[13,14] solar cells,[15] biomedical imaging,[16] and electrochemical biosensors.[17] Among them, bimetal (especially noble-metal-doped graphene) nanohybrids draw more attention, because they possess higher catalytic activity[18] and some special properties.[19] Now, 3D graphene-based bimetallic nanohybrids have an increasingly important role in the field of science for maximizing the accessibility to the supporter surface and metallic catalytic activity. Therefore, the simple and efficient preparation strategy for the novel 3D graphene-based bimetallic nanohybrids is highly desirable.

However, the reported methods for the preparation of 3D graphene structures are still limited, and most are compositions of graphene and substances,[20] such as carbon nanotubes[21] or polymer frameworks.[22] In addition, the reported preparation methods of 3D graphene-metal materials are complicated, especially for bimetallic anchored nanohybrids.[18,19] Those processes are almost step-by-step, which is time-consuming and complicated to perform. Meanwhile, some are achieved by using a large number of reducing agents (such as $NaHSO_3$, Na_2S, vitamin,

Received: September 16, 2014
Accepted: January 26, 2015
Published: January 26, 2015

DOI: 10.1021/am508540x
ACS Appl. Mater. Interfaces 2015, 7, 3480−3491

hydrogen iodide, and hydroquinone),[23] which limits large-scale preparation, because of the toxicity. Recently, many efforts have been made to fix the structure of the graphene network, such as developing a range of 3D graphene-based nanohybrids by spray drying, *in situ* spray pyrolysis or hydrothermal techniques.[24,25] Among them, the hydrothermal method is commonly used and found to be easy to handle. Shi et al.[25] demonstrate that graphene hydrogels, composed of a randomly cross-linked 3D graphene sheets network could be easily formed when a high concentration of a GO dispersion is hydrothermally reduced without the addition of any reducing agent. Subsequent researchers suggested that a 3D graphene-metal structure could be formed via a noble-metal-promoted self-assembly process,[8,12] which proposed a new path for synthesizing 3D nanohybrids. These outstanding works have been great inspirations for our current research. However, how to effectively inhibit the restacking and agglomeration of the GO sheets and simplify the preparation of nanohybrids with 3D structure without chemical or physical cross-linkers through one-step remains a challenge.

Given the problems above, we proposed the in situ synthesis strategy of self-assembled 3D reduced graphene oxide−magnetic palladium nanohybrids (3DRGO_Fe_3O_4-Pd) via the one-pot solvothermal reaction in ethylene glycol without the addition of a toxic reducing agent. During the preparation process, 3D graphene sheets and partial magnetite were used as supporters for the *in situ* growth of palladium nanoparticles, and L-glutamic acid served as a linker between palladium and magnetite nanoparticles.[18] Compared to other *in situ* or one-step methods,[12,26−30] in addition to being eco-friendly, our method has several prominent advantages:

(1) it is simple and easy to operate;
(2) Fe_3O_4 and Pd NPs have a small average size (8−10 nm) and are uniformly distributed on 3DRGO sheets; and
(3) the nanohybrids were reproducible, stable, and reusable.

After 10 cycles, the catalytic activity was still >90%, and the morphology and structure were basically unchanged; (4) 3DRGO_Fe_3O_4-Pd nanohybrids possess unique dual-enzyme activity and high affinity toward hydrogen peroxide (H_2O_2). Based on these features, the 3DRGO_Fe_3O_4-Pd nanohybrids have been successfully used as a novel mimetic peroxidase to develop a simple, highly sensitive and selective colorimetric method for the detection of H_2O_2, glutathione (GSH), and urine glucose for the first time.

EXPERIMENTAL SECTION

Materials. In this work, graphite powder and 3,3′,5,5′-tetramethylbenzidine (TMB) were purchased from Sigma−Aldrich. $PdCl_2$ was purchased from Shanghai Energy Chemicals Regent Co., Ltd. (Shanghai, China). L-glutamic acid, $FeCl_3{\cdot}6H_2O$, ethylene glycol, potassium permanganate, sodium acetate, glacial acetic acid, sodium dihydrogen phosphate, disodium hydrogen phosphate, urea, uric acid, and other regents were obtained from Tianjin Guangfu Chemical Reagent Factory (Tianjin, China). Glucose was purchased from Sangon Biotech Co., Ltd. (Shanghai). Glucose oxidase (GOx, 50 KU) was purchased from Sigma−Aldrich and stored in a refrigerator at −18 °C. Fructose, lactose, and maltose were obtained from Shanghai Zhongqin Chemical Reagent Company (Shanghai, China).

All chemicals were of analytical grade and were used as received without any further purification. Doubly distilled water was used throughout the work.

Instrumentation and Characterization. A Model TU-1901 double-beam ultraviolet−visible light (UV-vis) spectrophotometer (Beijing Purkine General Instrument Co. Ltd., China) was used to record absorption spectra and measure absorbance. A Hitachi Model 600 transmission electron microscopy (TEM) system and a high-resolution transmission electron microscopy (HRTEM) system was used to measure the morphologies of the nanohybrids and size of the nanoparticles. Scanning electron microscopy (SEM) images were acquired using a field-emission scanning electron microscopy system (Model S4800, Hitachi, Japan). X-ray diffraction (XRD) patterns of the nanohybrids were determined using a Rigaku D/Max-2400 X-ray diffractometer with Cu Kα radiation (λ = 0.154056). Fourier transform infrared (FT-IR) spectra were recorded on a Nicolet Nexus 670 Perkin−Elmer spectrometer. The chemical state of the coating surface was analyzed using X-ray photoelectron spectroscopy (XPS) (Perkin−Elmer, Model PHI-5702 multifunctional photoelectron spectrometer). A LDJ9600 Lakeshore Cryotronics 730 vibrating sample magnetometer (VSM) was used to research the magnetic property of nanohybrids. The specific surface area was measured using a multipoint Brunauer−Emmett−Teller (BET) technique (Model ASAP 2020, Micromeritics, USA), and the pore-size distribution was obtained using the Barrett−Joyner−Halenda (BJH) method. Raman spectra were recorded on a Dilor LABRAM-1B multichannel confocal microspectrometer. Element determination was measured using Perkin−Elmer Model 4300 DV inductively coupled plasma−atomic emission spectrometry (ICP-AES) equipment. Electron spin resonance (ESR) spectra were acquired using a Model JES-FA200 electron spin resonance spectrometer (JEOL). A Model CHI-660C electrochemical workstation (CH Instruments, Shanghai, China) was used for the measurements of electrochemical dc polarization. Freeze-drying was conducted on Scientz-12N vertical freeze-drying machine.

Synthesis of Graphene-Based Three-Dimensional Nanomaterials. Graphene oxide (GO) was synthesized via an improved method.[31]

The bimetallic loaded nanohybrids (3DRGO_Fe_3O_4-Pd) were synthesized according to the following procedure. The aqueous solutions of GO (10 mg mL^{-1}), L-glutamic acid, $FeCl_3{\cdot}6H_2O$, and $PdCl_2$ (8.87 mg mL^{-1}) were added stepwise into 15 mL of ethylene glycol (EG) by ultrasonic-assisted technology. Meanwhile, the pH value of the system was adjusted to 13.0 by adding NaOH solution dropwise under vigorous stirring, and continued to ultrasonic treatment for 0.5 h. Subsequently, the mixed solution was proceeded by ultrasound for 2 h to obtain a homogeneous suspension. Upon completion, the suspension was transferred into a Teflon-lined stainless-steel autoclave. The autoclave was sealed and heated at 180 °C for 12 h. After being air-cooled to room temperature, a columnar hydrogel was obtained. The product was washed with doubly distilled water several times, and lyophilization was applied to prevent the aggregation of graphene sheets during the drying process. Finally, Fe_3O_4 and Pd nanoparticles loaded three-dimensional reduced graphene oxide nanohybrids (3DRGO_Fe_3O_4-Pd) was obtained. The atomic molar ratio of Fe and Pd in the above nanohybrids is 1:1 analyzed by ICP-AES. To obtain the atomic ratio of Fe and Pd at 1:2 or 2:1, the quantity of $PdCl_2$ was fixed, and that of $FeCl_3{\cdot}6H_2O$ was changed accordingly.

3DRGO and monometallic loaded nanohybrids (3DRGO-Fe_3O_4 and 3DRGO-Pd) were prepared according to a process similar to that for 3DRGO_Fe_3O_4-Pd, and have been described in the Supporting Information.

Steady-State Kinetic Analysis of 3DRGO_Fe_3O_4-Pd as Peroxidase. The steady-state kinetic assays were carried out at 40 °C in 135 μL of reaction buffer (0.2 M HAc-NaAc, pH 4.0) with 60 μL of 1.0 mg mL^{-1} 3DRGO_Fe_3O_4-Pd, in the presence of H_2O_2 and TMB. The kinetic analysis of 3DRGO_Fe_3O_4-Pd with TMB as the substrate was performed by varying the concentrations of TMB at a fixed H_2O_2 concentration and vice versa. All the reactions were monitored at 652 nm. The reaction rates were then obtained by calculating the slopes of initial absorbance changes with time. All measurements were performed at least three times, and the values were averaged. Results were given as the mean ± the standard deviation (SD). Catalytic parameters were calculated by fitting data to the Michaelis−Menten equation (eq 1):

$$\frac{1}{\nu} = \frac{K_m}{V_m}\left(\frac{1}{[S]} + \frac{1}{K_m}\right) \quad (1)$$

DOI: 10.1021/am508540x
ACS Appl. Mater. Interfaces 2015, 7, 3480−3491

where v is the rate of conversion, V_m the maximum rate of conversion, [S] the substrate concentration, and K_m the Michaelis–Menten constant, which is equivalent to the substrate concentration, since the rate of conversion is half of V_m.

Assay Development Based on 3DRGO_Fe_3O_4–Pd Nanohybrids. The as-prepared 3DRGO_Fe_3O_4–Pd nanohybrids were used to catalyze the oxidation of a peroxidase substrate 3,3′,5,5′-tetramethylbenzidine (TMB) by H_2O_2 to produce a blue color product (see eq 2), which provides a colorimetric detection method for H_2O_2. Furthermore, this system has been applied to the detection of the analytes that can consume or produce H_2O_2. Through combination of the catalytic reaction of glucose with glucose oxidase (GOx) (eq 3) and the nanohybrids catalytic reaction (eq 2), a colorimetric method for glucose detection was developed. Reduced GSH, which is converted to its oxidative form (GSSG) by H_2O_2 (eq 4), can consume H_2O_2 and result in the shallowing color of the nanohybrid–TMB–H_2O_2 system.

$$H_2O_2 + \text{TMB} \xrightarrow{\text{nanohybrids}} 2H_2O + \text{oxidized TMB} \quad (2)$$

$$O_2 + \text{glucose} \xrightarrow{\text{GOx}} H_2O_2 + \text{gluconic acid} \quad (3)$$

$$H_2O_2 + 2\text{GSH} \rightarrow 2H_2O + \text{GSSG} \quad (4)$$

For glucose detection, the procedure was shown as follows:

(1) 10 μL of 1 mg mL^{-1} GOx and 100 μL of glucose with different concentrations in a 5 mM phosphate buffer (pH 7.0) were incubated at 37 °C for 30 min; and

(2) 72 μL of the above glucose reaction solutions was mixed with 100 μL of 0.2 M HAc–NaAc buffer (pH 4.0), 24 μL of 20 mM TMB and 60 μL of 1.0 mg mL^{-1} 3DRGO_Fe_3O_4-Pd for another 10 min of incubation at 40 °C.

Then, the mixture was placed into an ice bath for 10 min, and 200 μL of the supernatant was taken out and diluted with doubly distilled water to 3 mL. Finally, the absorbance at 652 nm was obtained. In control experiments, maltose, lactose, fructose, uric acid, urea, K^+, and Cl^- were used as interferences for the test.

The urine sample with diabetes, provided by a male volunteer from the First Affiliated Hospital of Lanzhou University, was first treated by centrifugation. The obtained supernatant was diluted by a factor of 10 with 5 mM phosphate buffer (pH 7.0). One hundred microliters (100 μL) of the diluted filtrate was used to detect glucose, as described in the above procedure.

The detection procedures of H_2O_2 and reduced GSH were provided in the Supporting Information.

RESULTS AND DISCUSSION

1. Characterization of 3DRGO_Fe_3O_4-Pd. Briefly, a facile one-pot solvothermal strategy was developed to fabricate the 3DRGO nanohybrids with *in situ*-formed Fe_3O_4 and Pd nanoparticles (NPs) on it. The entire process is shown in Scheme 1. First, L-glutamic acid was added into graphene solution and, with ultrasonic assistance, the partial self-assembly of graphene occurred. Then with the addition of ferric chloride into ethylene glycol, 3D graphene structure was formed by a metal ion induced self-assembly process,[12] followed by mixing with palladium chloride. In an alkaline environment (pH 13), ferrum and palladium existed as hydroxide in graphene solution. After thermal reduction in the ethylene glycol, further self-assembling of graphene occurred. Meanwhile, Fe_3O_4 and Pd NPs were grown on 3DRGO, and a part of Pd NPs were also loaded on Fe_3O_4 NPs using L-glutamic acid as linkers.[18] The effect of the molar ratio of Fe and Pd at 1:2, 1:1, and 2:1, respectively, on morphology and distribution of nanoparticles on the 3DRGO was first examined, and finally 1:1 was chosen as the optimal ratio.

Figures 1A and 1B show the SEM images of the 3DRGO_Fe_3O_4-Pd nanohybrids. It was easily found that the interconnected 3D porous network of graphene sheets was well-defined (Figure 1A), and some nanoparticles were located on the surface of 3D graphene sheets uniformly (Figure 1B). Comparing the TEM image of 3DRGO_Fe_3O_4-Pd (Figure 1C) with those of GO (see Figure S1A in the Supporting Information) and 3DRGO (see Figure S1B in the Supporting Information), it was confirmed that uniformly sized nanoparticles were successfully anchored onto the 3DRGO sheets via a one-pot solvothermal strategy, and their average diameter was ~8–10 nm (see Figure S2

Scheme 1. Schematic of the Preparation Process for 3DRGO_Fe_3O_4-Pd Nanohybrids

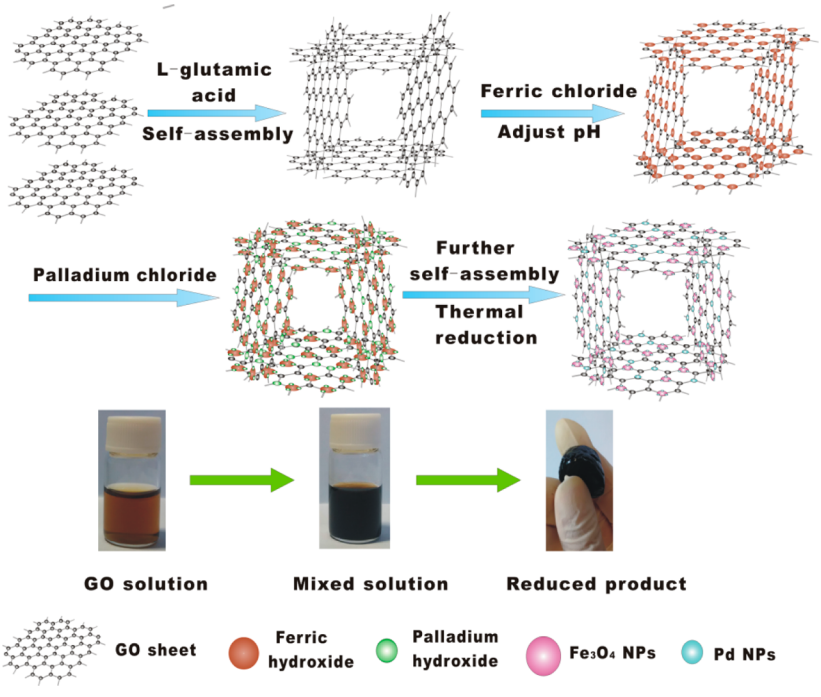

DOI: 10.1021/am508540x
ACS Appl. Mater. Interfaces 2015, 7, 3480–3491

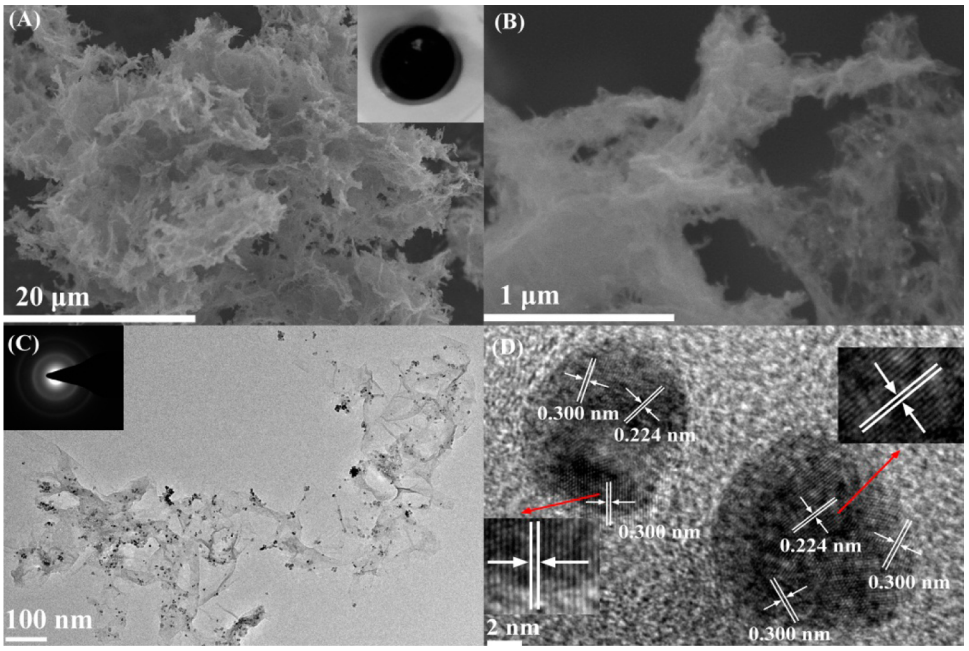

Figure 1. (A, B) SEM images of the 3DRGO_Fe_3O_4-Pd; inset in panel (A) is a photograph of the obtained nanohybrids. (C) TEM images of 3DRGO_Fe_3O_4-Pd; inset shows the SAED pattern of the corresponding nanohybrids. (D) HRTEM image of Pd and Fe_3O_4 NPs on 3DRGO.

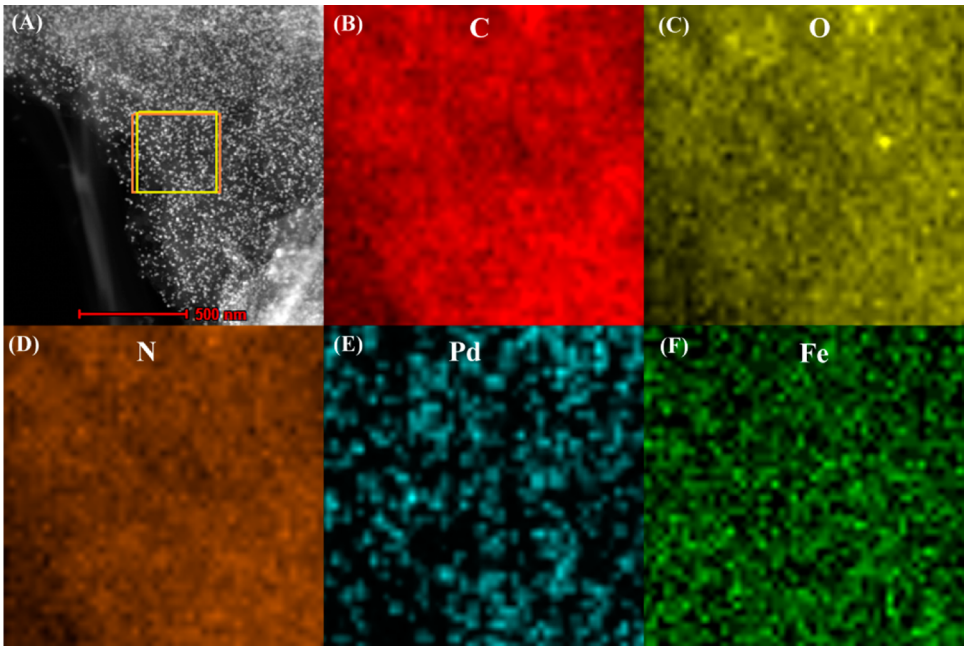

Figure 2. (A) Dark-field STEM images of 3DRGO_Fe_3O_4-Pd nanohybrids; (B–F) corresponding elemental mappings of component elements ((B) C, (C) O, (D) N, (E) Pd, and (F) Fe).

in the Supporting Information). Even after the ultrasonication for preparation of the TEM sample, these nanoparticles were still firmly anchored onto the 3D graphene sheets. Figure 1D and Figure S3 in the Supporting Information show the HRTEM image of the nanoparticles anchored onto the 3DRGO sheets. Two types of spacing of the lattice fringes could be clearly observed; these are (1) 0.224 nm, which corresponds to the Pd (111) crystalline planes;[32] and (2) 0.300 nm, which is in good agreement with the (220) planes of Fe_3O_4 NPs.[33] As suggested above, those nanoparticles grown on 3DRGO sheets are Pd and Fe_3O_4 NPs, respectively. The elemental mappings (Figure 2) and EDS results (Figure S4 in the Supporting Information) also reveal that Pd and Fe elements coexist on the 3DRGO sheets, which are quite consistent with HRTEM analysis.

The XRD patterns of the bimetallic 3DRGO_Fe_3O_4–Pd nanohybrids was verified by comparing with those of original graphite and GO (Figure 3A); monometallic 3DRGO_Pd and 3DRGO_Fe_3O_4 nanohybrids synthesized under the similar conditions (Figure 3B). The broad peak located in the range of 15°–30° is assigned to the (002) plane of stacked graphene network within 3D porous structure.[25] A series of typical peaks at 40.4°, 47.0°, 68.6°, 82.7°, and 87.3° correspond to the (111), (200), (220), (311), and (322) planes of the standard face-centered-cubic (fcc) Pd NPs (JCPDS Powder Diffraction File

DOI: 10.1021/am508540x
ACS Appl. Mater. Interfaces 2015, 7, 3480–3491

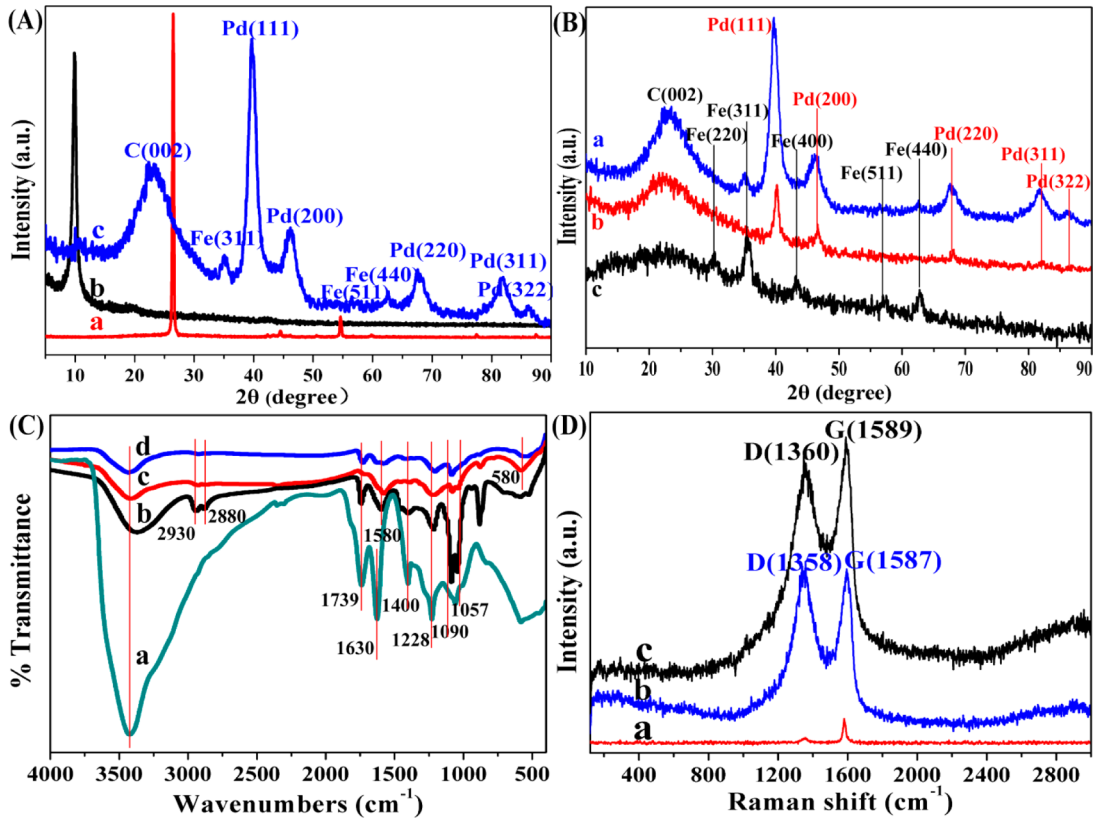

Figure 3. (A) XRD patterns of nanohybrids: graphite (spectrum a), GO (spectrum b), and 3DRGO_Fe_3O_4-Pd (spectrum c). (B) XRD patterns of different nanohybrids: 3DRGO_Fe_3O_4-Pd (spectrum a), 3DRGO_Pd (spectrum b), and 3DRGO_Fe_3O_4 (spectrum c). (C) FTIR spectra: GO (spectrum a), 3DRGO_Pd (spectrum b), 3DRGO_Fe_3O_4 (spectrum c), and 3DRGO_Fe_3O_4-Pd (spectrum d). (D) Raman spectra: graphite (spectrum a), 3DRGO_Fe_3O_4-Pd (spectrum b), and GO (spectrum c).

No. 87-0645). The peaks at 30.1°, 35.5°, 43.1°, 57.1°, and 62.7° correspond to the (220), (311), (400), (511), and (440) planes of the standard fcc Fe_3O_4 NPs (JCPDS Powder Diffraction File No. 88-0315). The results are consistent with lattice spacing data. Summing up the above, the Pd and Fe_3O_4 NPs were anchored on the 3D graphene structure.

Furthermore, X-ray photoelectron spectroscopy (XPS) measurement was also used to elucidate the composition and surface oxidation states of the as-prepared materials, as shown in Figure 4. The two peaks centered at 335.4 and 340.8 eV (Figure 4B) can be assigned to Pd $3d_{5/2}$ and Pd $3d_{3/2}$, respectively,[34] indicating the presence of Pd in a metallic state almost without surface oxidation.[35] Moreover, the Fe 2p binding energies of 710.5 and 723.8 eV (Figure 4C) confirm the oxidation state of Fe_3O_4 in the hybrid material.[36] The nanohybrids obtained after solvothermal reduction has a markedly decreased relative contribution of the C 1s components associated with oxygenated functional groups compared with the original GO (Figures 4D and 4E). After the solvothermal reduction, the oxygen species of C−O−C (hydroxyl and epoxy, 286.8 eV) and C═O (carbonyl, 287.8 eV) of GO reduced significantly, indicating an efficient deoxygenation of GO partially occurred in the reaction.[37,38] The major remaining species in 3DRGO_Fe_3O_4−Pd nanohybrids were C−C (284.6 eV) and C−OH (286.0 eV), these residual oxygen-containing functional groups could also capture metal ions for *in situ* synthesis of metal nanoparticles on RGO sheets. Hence, Pd NPs can not only selectively deposit on magnetite, but also disperse on the RGO sheets corresponding to Figure S3 in the Supporting Information.[18]

To further prove the reduction of GO, the FTIR spectra were measured. As shown in Figure 3C, the peaks at 1739, 1400, and 1228 cm^{-1} are attributed to C═O, C−O, and −OH of the −COOH groups, respectively. Meanwhile, the bands at 580 cm^{-1} in curves c and d are the characteristic stretching vibrations of Fe−O.[39] In curves b−d, the peak intensities of oxygenated functional groups of the nanohybrids materials decreased dramatically compared with the original GO. Hence, deoxygenation of GO partially occurred in the solvothermal reaction. This point can also be demonstrated by Raman spectra of GO and 3DRGO_Fe_3O_4−Pd nanohybrids (Figure 3D). The two prominent peaks at 1360 and 1589 cm^{-1} are the characteristic peaks of D and G bands from GO. The decrease in the ratio of the intensities of the G and D bands (I_G/I_D) of nanohybrids is an indication of the reduction of GO.[40] Furthermore, compared to the pure GO, the shift of the peaks can be found for both D and G bands, indicating a significant charge transfer between the graphene nanosheets and the nanoparticles on them,[41] which is helpful for improving its catalytic performance.[7]

The BET isotherm (see Figure S6 in the Supporting Information) appears to be categorized as a Type IV isotherm. The hysteresis loop seems to be Type B associated with slit-shaped pores, which makes sense, because of the flakelike structure of GO.[42] This was revealed in the low- and high-resolution SEM images shown in Figures 1A and B, indicating the porosity of 3DRGO sheets. The nanohybrids have an average BET surface area of 194 $m^2\ g^{-1}$. The surface area is relatively low, compared to some graphene aerogel, which may result from different post-treatment methods. Generally, treatment by supercritical CO_2 results in higher surface area (500−1200 $m^2\ g^{-1}$),[43]

DOI: 10.1021/am508540x
ACS Appl. Mater. Interfaces 2015, 7, 3480−3491

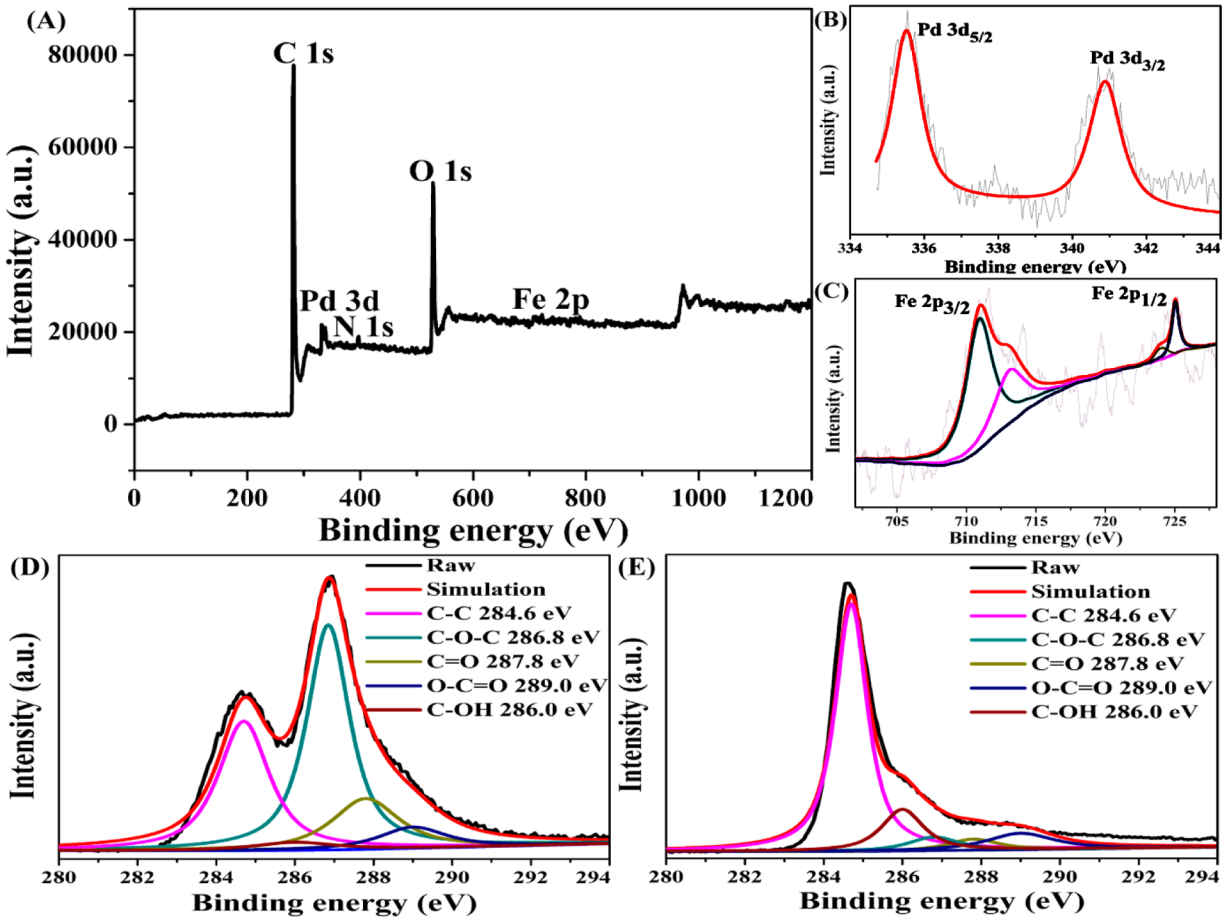

Figure 4. (A) XPS spectra of survey scan of 3DRGO_Fe_3O_4-Pd nanohybrids; (B) high-resolution Pd 3d XPS spectra of materials; (C) high-resolution Fe 2p XPS spectra of materials; (D) high-resolution C 1s XPS spectra of GO; and (E) high-resolution C 1s XPS spectra of 3DRGO_Fe_3O_4-Pd.

while freeze-drying or direct drying by heating leads to low values (<200 m^2 g^{-1}).[44,45] Moreover, this material has a centralized distribution of mesopores, and the adsorption average pore width is ~3.5 nm, identified from the pore distribution histogram of the inset in Figure S6 in the Supporting Information. Compared with other similar pure 3DRGO structures formed by cross-linkers,[42] this material shows a relatively narrow size distribution, primarily because of the following two reasons:

(1) There are many nanoparticles loaded on the 3DRGO sheets, whose average diameter is ~8−10 nm and, hence, some of the holes were possibly covered; and
(2) the monolithic materials were ground to a powder for BET measurement, and the bulk of macropores are likely to be lost.

However, the BET data could truly indicate the character of the materials in its following applications.

The magnetization curve of 3DRGO_Fe_3O_4−Pd (see Figure S7 in the Supporting Information) shows no remanence or coercivity at room temperature (inset in Figure S7b in the Supporting Information), suggesting that the magnetic nanohybrids are superparamagnetic. The saturation magnetization is 7.6 emu g^{-1}, and the inset in Figure S7a in the Supporting Information demonstrates that it only takes several seconds to collect 3DRGO_Fe_3O_4−Pd from aqueous solution with a magnet, which makes it possible to realize separation of the catalyst from the mixed solutions.

2. Enzyme Mimetic Activity of 3DRGO_Fe_3O_4-Pd.

2.1. Dual-Enzyme Activity. To demonstrate the enzyme mimetic activity of the 3DRGO_Fe_3O_4-Pd nanohybrids, the typical peroxidase substrate 3,3′,5,5′-tetramethylbenzidine (TMB) was chosen as the chromogenic substrate, which are shown in Figure 5A. Even without H_2O_2 in the system, the material could still catalytically oxidize the TMB substrate to display a light blue color (see Figure 5A, curve b). Namely, the 3DRGO_Fe_3O_4-Pd nanohybrids exhibited oxidase-like activity,[46] demonstrated by an electrochemical dc polarization method, as shown in Figure 5B. Compared to bare electrode, the modified electrode presents a relatively negative balance potential and high current. This fact indicates that the modified electrode reacts more easily with TMB,[47] which means that TMB can be oxidized by the 3DRGO_Fe_3O_4−Pd nanohybrids, even in the absence of H_2O_2.

Meanwhile, the 3DRGO_Fe_3O_4-Pd + TMB + H_2O_2 system produced a deep blue color (Figure 5A, curve c), which demonstrated that the nanohybrids behave similar to peroxidase. Peroxidase can degrade H_2O_2 to produce hydroxyl radicals (·OH), which are then responsible for substrate oxidation.[48] We first confirm the ·OH formation by adding the terephthalic acid into the H_2O_2 + 3DRGO_Fe_3O_4-Pd system, in which terephthalic acid could react with •OH easily to form fluorescent 2-hydroxy terephthalic acid.[49] As shown in Figure 5C, it is clearly shown that the fluorescence intensity gradually increases as the dosage of the catalyst increases (curves a−e: 0, 0.03, 0.06, 0.09, and 0.12 mg mL^{-1} 3DRGO_Fe_3O_4-Pd), suggesting the increasing amount of generated •OH. Electron spin resonance

DOI: 10.1021/am508540x
ACS Appl. Mater. Interfaces 2015, 7, 3480−3491

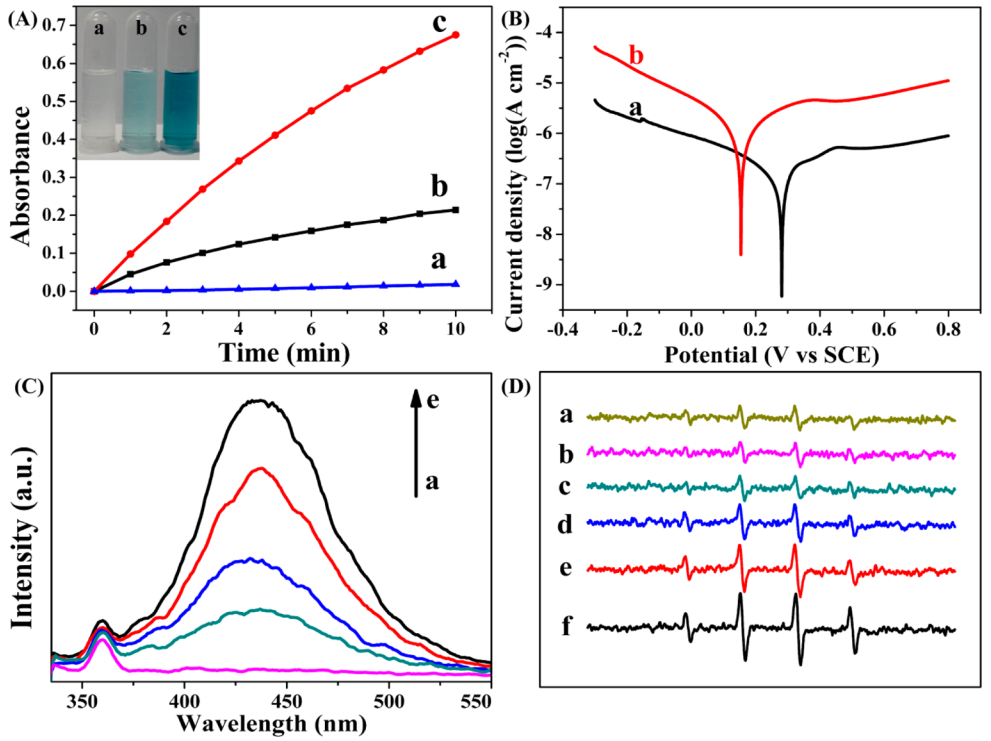

Figure 5. (A) Time-dependent absorbance changes at 652 nm of TMB in different reaction systems: TMB + H_2O_2 (curve a), 3DRGO_Fe_3O_4-Pd + TMB (curve b), and 3DRGO_Fe_3O_4-Pd + TMB + H_2O_2 (curve c). (B) Polarization curves of bare electrode (curve a) and modified electrode (curve b) with 3DRGO_Fe_3O_4-Pd in the TMB aqueous solution; scan rate was 2 mV s^{-1}. (C) Effect of the 3DRGO_Fe_3O_4-Pd dosage on the formation of hydroxyl radical in H_2O_2 aqueous solution with terephthalic acid as a fluorescence probe. (D) Effect of the 3DRGO_Fe_3O_4-Pd dosage on the DMPO spin-trapping EPR measurements.

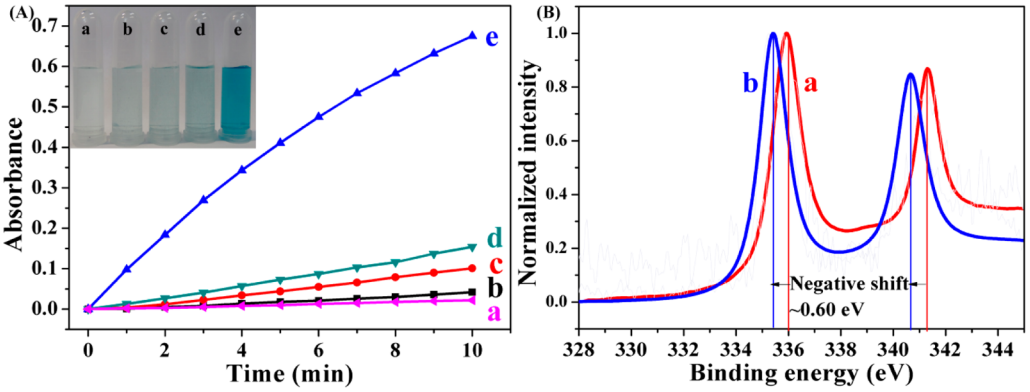

Figure 6. (A) Time-dependent absorbance changes at 652 nm of TMB using different catalysts: 3DRGO (curve a), 3DRGO_Fe_3O_4 (curve b), 3DRGO_Pd (curve c), physical mixture of curves b and c (curve d), and 3DRGO_Fe_3O_4-Pd (curve e). Inset shows the color change of different samples, respectively. (B) Pd_{3d} XPS spectra of 3DRGO_Pd (curve a) and 3DRGO_Fe_3O_4-Pd (curve b).

spectroscopy (ESR) is the most powerful and direct analytical method for quantification of short-lived radicals.[50] Figure 5D shows the spectra of 5,5-dimethyl-1-pyrroline *N*-oxide DMPO/•OH in the ESR measurement (curves a–f: 0, 0.02, 0.04, 0.08, 0.12, and 0.16 mg mL^{-1} 3DRGO_Fe_3O_4-Pd nanohybrids, respectively), revealing the •OH formation in H_2O_2 solution through the adding of 3DRGO_Fe_3O_4-Pd and the amount of free radical is proportional to the dosage of the catalyst. These results indicate that 3DRGO_Fe_3O_4–Pd possesses the catalytic ability to decompose H_2O_2 to generate •OH radical, which certificated the peroxidase-like activity of the nanohybrids.

To further prove the high peroxidase-like activity of the bimetallic-loaded 3DRGO_Fe_3O_4-Pd nanohybrids, the monometallic nanohybrids (3DRGO_Fe_3O_4 and 3DRGO-Pd) with the similar morphology and size distribution as 3DRGO_Fe_3O_4-Pd (seen in Figure S5 in the Supporting Information) are synthesized via the similar one-pot solvothermal method (the synthetic process described in the Supporting Information) and used as a catalyst in the TMB–H_2O_2 system. The experimental conditions, including the amount of three types of nanohybrids, are the same. As revealed in Figure 6A, 3DRGO showed very weak catalytic performance (curve a). After loading some Fe_3O_4 NPs (curve b) or Pd NPs (curve c), the catalytic performance of 3DRGO was obviously improved. However, neither of two monometallic nanohybrids exhibited better catalytic capability than bimetallic 3DRGO_Fe_3O_4-Pd (curve e). Even for their physical mixture (curve d), the catalytic capability reached the sum of two monometallic nanohybids, but was less than a quarter of the catalytic

DOI: 10.1021/am508540x
ACS Appl. Mater. Interfaces 2015, 7, 3480–3491

capability of 3DRGO_Fe_3O_4-Pd. This is probably due to the easy capture and immobilization for H_2O_2 on the three-dimensional porous structure, and more importantly, the synergistic effect of Pd NPs and Fe_3O_4 NPs through the electron transfer.[27,51] In order to demonstrate this point, electronic structures of Pd in 3DRGO_Pd and 3DRGO_Fe_3O_4-Pd were characterized by XPS measurements (Figure 6B). The electron binding energy of the 3DRGO_Fe_3O_4-Pd was decreased by ~0.60 eV compared with that of 3DRGO_Pd (C 1s set to 284.6 eV for calibration). Such negative shift implies electron transfer from Fe_3O_4 to Pd NPs,[19,49] which may offer more enhanced catalysis for oxidation of TMB. Meanwhile, the work function was 5.60 eV for Pd(111)[52] and 5.52 eV for Fe_3O_4(111),[27,53] this difference could also promote electron transfer from Fe_3O_4 to Pd NPs to improve the catalytic ability of the nanohybrids. Therefore, in the study, 3DRGO acts as the supporter and site of electronic transfer,[54] Pd NPs mainly behave as a highly efficient catalyst, and Fe_3O_4 NPs play the mixed role of catalyst in the TMB−H_2O_2 system and supporter for Pd NPs.[18] Furthermore, the effect of the atomic ratio of Fe and Pd at values of 1:1, 1:2, and 2:1 on the catalytic activity of the nanohybrids was examined (see Figure S8 in the Supporting Information). Keeping the total mass of the three nanohybrids the same, there are too few Fe_3O_4 NPs for it to act as a good supporter for Pd NPs at 1:2, and there are too few Pd NPs to provide effective catalysis at a ratio of 2:1. In other words, the amount of Pd NPs, especially those deposited on magnetite, is crucial to the catalytic activity of the nanohybrids. This is also proof of the synergistic effect between metals loaded on support.

The dual-enzyme mimetic activity of 3DRGO_Fe_3O_4-Pd nanohybrids is displayed in Scheme S1 of the Supporting Information: the peroxidase-like activity is much higher than oxidase-like activity. Furthermore, the peroxidase-like character is exploited for H_2O_2, GSH, and glucose determination in the following applications.

2.2. Steady-State Kinetic Assay of the Peroxidase-Like Activity. Similar to HRP, the catalytic activity of 3DRGO_Fe_3O_4-Pd nanohybrids is dependent on the pH, temperature, H_2O_2 concentration, and catalyst dosage (see Figure S9 in the Supporting Information). In order to eliminate the breakdown of H_2O_2 from possible Fenton's reagent,[55] 3DRGO_Fe_3O_4-Pd are incubated with reaction buffer solution (pH 4.0) for 12 h. The amount of iron ions in the supernatant was detected by ICP-AES and is lower than 1% (w/w). Furthermore, compared to 3DRGO_Fe_3O_4-Pd under the same conditions, the supernatant has no obvious catalytic activity (see Figure S10 in the Supporting Information). These results confirmed that the high peroxidase-like activity was evolved from the 3DRGO_Fe_3O_4−Pd nanohybrids themselves, instead of leaching Fe ions.

For further investigating the peroxidase-like catalytic mechanism, the apparent steady-state kinetic parameters for this reaction were determined. Typical Michaelis−Menten curves can be obtained for 3DRGO_Fe_3O_4-Pd nanohybrids within the suitable concentration ranges of TMB (Figure S11A in the Supporting Information) and H_2O_2 (Figure S11B in the Supporting Information). The maximum initial velocity (V_m) and Michaelis−Menten constant (K_m) are calculated from Lineweaver−Burk plots. The calculated values for 3DRGO_Fe_3O_4-Pd nanohybrids and other catalysts, as well as HRP, are listed in Table S1 in the Supporting Information. By comparing the apparent kinetic parameters, the K_m value of 3DRGO_Fe_3O_4-Pd nanohybrids with H_2O_2 as the substrate was 2 orders of magnitude lower than those of GO and HRP, and at least 30 times lower than those of other nanomaterials, such as GO-Fe_3O_4, suggesting that the incorporation of Pd and Fe_3O_4 NPs on 3DRGO sheets notably improve the catalytic affinity toward H_2O_2.[56] This result is in agreement with the fact that a lower H_2O_2 concentration is required for the 3DRGO_Fe_3O_4-Pd nanohybrids when maximum activity is obtained. Furthermore, the double reciprocal plots of velocity against the concentration of one substrate were also acquired. As can be seen in Figures S11C and S11D in the Supporting Information, the double-reciprocal plots revealed the characteristic parallel lines of a ping-pong mechanism.[57,58]

3. Real Application of the Proposed Method. *3.1. Analysis Performance.* Based on the high affinity and catalytic activity of 3DRGO_Fe_3O_4-Pd nanohybrids to H_2O_2, a simple colorimetric method is developed to detect H_2O_2 using the TMB system. Figure 7A shows typical H_2O_2 concentration−response curves under the optimum conditions. The linear range for H_2O_2 is from 0.5 μM to 30 μM with detection limits of detection (LODs) of 8.6×10^{-8} M, which is comparative to and even more sensitive than other graphene-based nanohybrids (as shown in Table S2 in the Supporting Information). Furthermore, this system was applied to the detection of the analytes that could consume or produce H_2O_2. GSH, which plays a crucial role in cellular resistance against oxidative damage, can consume H_2O_2 and result in the shallowing color of the nanohybrid−TMB−H_2O_2 system. Based on the combination of the 3DRGO_Fe_3O_4-Pd nanohybrid catalytic reaction with the conversion of GSH to its oxidative forms (GSSH), a new colorimetric detection for GSH was developed. The linear range for GSH is from 0.4 μM to 40 μM with LODs of 5.2×10^{-8} M, as shown in Figure 7B. Moreover, H_2O_2 is the main product of the glucose oxidase (GOx)-catalyzed reaction; therefore, we made further efforts to detect glucose using H_2O_2 as media. Figure 7C shows typical glucose concentration−response curves with the linear range of 0.5−60 μM and LODs of 1.3×10^{-7} M. This colorimetric method, which is based on 3DRGO_Fe_3O_4-Pd nanohybrids gives lower LODs for glucose than other methods using nanoparticle-based materials as a catalyst (shown in Table S3 in the Supporting Information). The high sensitivity may be attributed to the presence of a 3D structure and bimetal load in the nanohybrids, where there are many mesopores to capture H_2O_2 and catalyze its decomposition easily.

The proposed one-pot solvothermal method for preparing 3DRGO_Fe_3O_4−Pd nanohybrids was simple, robust, and reproducible. As shown in Table S4 in the Supporting Information, the reproducibility among six batches of the prepared nanohybrids is <3%. Even after one month of storage, >90% catalytic activity of the 3DRGO_Fe_3O_4−Pd is maintained (see Figure S12 in the Supporting Information), showing their high stability during long-term storage. The reusability of the nanohybrids was also evaluated and shown in Figure 8. After 10 cycles, the catalytic activity was still >90%, and the morphology and structure were basically unchanged. Therefore, 3DRGO_Fe_3O_4-Pd nanohybrids possess good stability and high catalytic activity.

3.2. Detection of Urine Glucose. To demonstrate the feasibility of this proposed method for practical applications, the analysis of urine glucose of the diabetes was carried out. Prior to the sample test, the selectivity of this colorimetric method was first evaluated. Several types of interferences widely existing in human urine, including KCl, uric acid (UA), urea, and other similar sugars (such as fructose, lactose, and maltose), are tested.[59] As expected (see Figure 9A), fructose, lactose, and maltose gave negligible responses, compared to glucose, and even the concentration (850 μM) of these interferences was much higher than that of glucose (85 μM). The high selectivity was attributed to the specific recognition of GOx. Furthermore, KCl and urea, the concentrations of which were 25-fold higher

DOI: 10.1021/am508540x
ACS Appl. Mater. Interfaces 2015, 7, 3480−3491

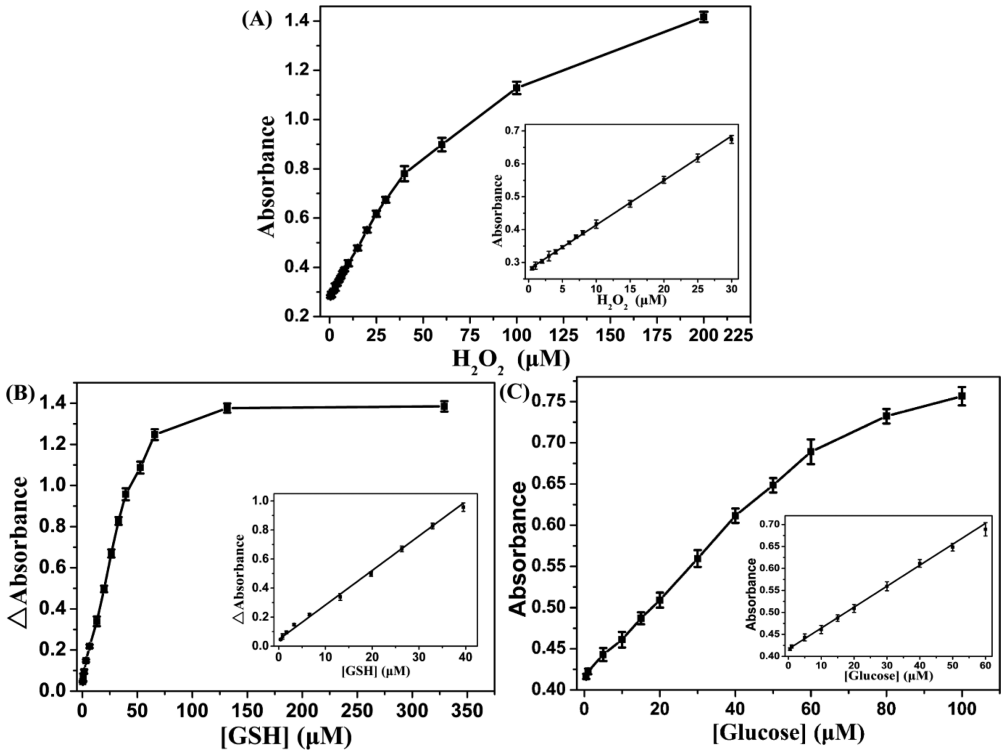

Figure 7. Dose−response curve for (A) H_2O_2, (B) GSH ($\Delta A = A_{blank} - A_{GSH}$), and (C) glucose detection at 652 nm under the optimum conditions; insets show their respective linear calibration plots. The error bars represent the standard deviation of six measurements.

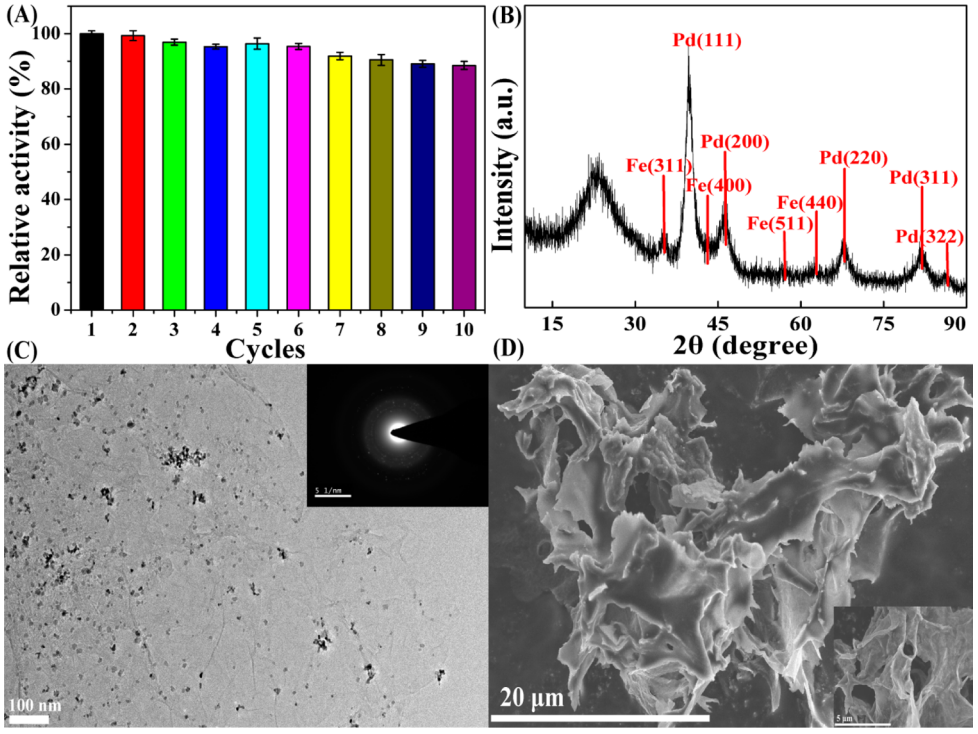

Figure 8. (A) Reusability performance of 3DRGO_Fe_3O_4-Pd nanohybrids for 10 cycles; (B) XRD pattern, (C) TEM image, and (D) SEM image of the nanohybrids after 10 cycles. The inset in panel (C) shows the SAED pattern of the corresponding nanohybrids, and the inset in panel (D) is the partial, enlarged view.

than that of glucose, did not interfere with the detection of glucose. Uric acid (UA), as a reducing agent, would consume H_2O_2 and decrease the absorbance of the system if it had the same concentration as glucose (Figure 9B). However, after a factor-of-10 dilution with phosphate buffer, the content of uric acid was largely decreased, and the molar ratio of glucose and uric acid in the urine of diabetes was commonly higher than 1:1.[60,61] Therefore, the interference from uric acid was also negligible.

DOI: 10.1021/am508540x
ACS Appl. Mater. Interfaces 2015, 7, 3480−3491

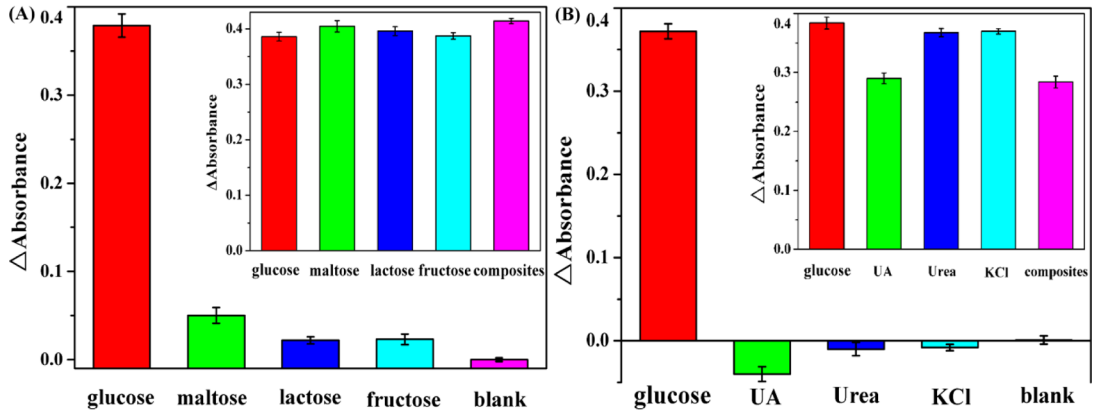

Figure 9. Selectivity study for glucose detection by monitoring the absorbance change at 652 nm ($\Delta A = A_{total} - A_{blank}$) upon the addition of (A) various sugars and the mixtures of sugars and (B) some common substances as interferences. The insets in panels (A) and (B) show the anti-interference study in the coexistence of glucose. The concentrations of the analytes were as follows: glucose, 85 μM; maltose, lactose, and fructose, 850 μM; UA, 85 μM; and urea and KCl, 2.1 mM.

These results indicate that our colorimetric method based on the nanohybrids catalyst shows high selectivity to glucose sensing against other coexisting disrupters.

The nanohybrids and the GOx-based colorimetric method was employed to detect glucose in the diluted urine sample. The analytical results are summarized in Table S5 in the Supporting Information. It can be seen that the proposed colorimetric method exhibited exact recovery results (98.0%−102.0%). The concentration of glucose in urine was determined as 6.8 mM (72.9 mg dL^{-1}). The urine test is positive when the amount of glucose is more than 50−100 mg dL^{-1}.[61] Therefore, this colorimetric method is applicable to determine glucose in urine sample, and it can also be applied to detect other substances using hydrogen peroxide as media, which is important for biological and biomedical applications.

CONCLUSION

In summary, an *in situ* synthesis method of 3DRGO_Fe_3O_4-Pd nanohybrids through a one-pot strategy was provided, and these nanohybrids possess good stability and high catalytic activity. During the synthesis process, three-dimensional (3D) graphene and partial magnetite are used as supporters for the *in situ* growth of palladium NPs on them, and L-glutamic acid serves as the linker between magnetite and palladium NPs. Furthermore, the 3DRGO_Fe_3O_4-Pd nanohybrids was found to have intrinsic dual-enzyme activity for the first time. Comparing to HRP and some other peroxidase nanomimetics, 3DRGO_Fe_3O_4-Pd nanohybrids shows two outstanding advantages as a novel mimic peroxidase: high catalytic efficiency and high affinity toward substrate H_2O_2 on account of the synergies of both metals probably. Based on these, a simple, highly sensitive and selective method for the colorimetric detection of reduced glutathione (GSH) and urine glucose was provided. This work will facilitate the utilization of intrinsic dual-enzyme activity and other catalytic properties of 3DRGO_Fe_3O_4−Pd nanohybrids in environmental chemistry, biotechnology, and medicine.

ASSOCIATED CONTENT

Supporting Information

Synthesis procedure for 3DRGO, 3DRGO_Fe_3O_4, 3DRGO_Pd; determination of the optimization condition; general procedures for H_2O_2 and GSH colorimetric detection; obtention of standard curve for glucose; determination of reusability. Additional TEM, EDS, material stability, and steady-state kinetic assay figures. This material is available free of charge via the Internet at http://pubs.acs.org/.

AUTHOR INFORMATION

Corresponding Author

*E-mail address: hlchen@lzu.edu.cn.

Notes

The authors declare no competing financial interest.

ACKNOWLEDGMENTS

This work was financially supported by National Nature Science Foundation of China (No. 21475053).

REFERENCES

(1) Novoselov, K. S.; Geim, A. K.; Morozov, S. V.; Jiang, D.; Zhang, Y.; Dubonos, S. V.; Grigorieva, I. V.; Firsov, A. A. Electric field Effect in Atomically Thin Carbon Films. *Science* **2004**, *306*, 666−669.

(2) Rao, C. N. R.; Sood, A. K.; Subrahmanyam, K. S.; Govindaraj, A. Graphene: The New Two-Dimensional Nanomaterial. *Angew. Chem., Int. Ed.* **2009**, *48*, 7752−7777.

(3) Allen, M. J.; Tung, V. C.; Kaner, R. B. Honeycomb Carbon: A Review of Graphene. *Chem. Rev.* **2010**, *110*, 132−145.

(4) Xu, C.; Wang, X.; Zhu, J. W. Graphene-Metal Particle Nanocomposites. *J. Phys. Chem. C* **2008**, *112*, 19841−19845.

(5) Park, S.; Shao, Y. Y.; Wan, H. Y.; Rieke, P. C.; Viswanathan, V. V.; Towne, S. A.; Saraf, L. V.; Liu, J.; Lin, Y. H.; Wang, Y. Design of Graphene Sheets-Supported Pt Catalyst Layer in PEM Fuel Cells. *Electrochem. Commun.* **2011**, *13*, 258−261.

(6) Yu, D. S.; Dai, L. M. Self-Assembled Graphene/Carbon Nanotube Hybrid Films for Supercapacitors. *J. Phys. Chem. Lett.* **2010**, *1*, 467−470.

(7) Chen, W. F.; Li, S. R.; Chen, C. H.; Yan, L. F. Self-Assembly and Embedding of Nanoparticles by In Situ Reduced Graphene for Preparation of a 3D Graphene/Nanoparticle Aerogel. *Adv. Mater.* **2011**, *23*, 5679−5683.

(8) Tang, Z. H.; Shen, S. L.; Zhuang, J.; Wang, X. Noble-Metal-Promoted Three-Dimensional Macroassembly of Single-Layered Graphene Oxide. *Angew. Chem., Int. Ed.* **2010**, *122*, 4603−4607.

(9) Sridhar, V.; Kim, H. J.; Jung, J. H.; Lee, C.; Park, S.; Oh, I. K. Defect-Engineered Three-Dimensional Graphene-Nanotube-Palladium Nanostructures with Ultrahigh Capacitance. *ACS Nano* **2012**, *6*, 10562−10570.

(10) Kim, Y. K.; Min, D. H. Durable Large-Area Thin Films of Graphene/Carbon Nanotube Double Layers as a Transparent Electrode. *Langmuir* **2009**, *25*, 11302−11306.

DOI: 10.1021/am508540x
ACS Appl. Mater. Interfaces 2015, 7, 3480−3491

(11) He, H. Y.; Li, X. L.; Wang, J.; Qiu, T. F.; Fang, Y.; Song, Q.; Luo, B.; Zhang, X. F.; Zhi, L. J. Reduced Graphene Oxide Nanoribbon Networks: A Novel Approach towards Scalable Fabrication of Transparent Conductive Films. *Small* **2013**, *9*, 820−824.
(12) Chang, Y. H.; Li, J.; Wang, B.; Luo, H.; He, H. Y.; Song, Q.; Zhi, L. J. Synthesis of 3D Nitrogen-Doped Graphene/Fe_3O_4 by a Metal Ion Induced Self-Assembly Process for High-Performance Li-ion Batteries. *J. Mater. Chem. A* **2013**, *1*, 14658−14665.
(13) Li, Z. F.; Zhang, H. Y.; Liu, Q.; Sun, L. L.; Stanciu, L.; Xie, J. Fabrication of High-Surface-Area Graphene/Polyaniline Nanocomposites and Their Application in Supercapacitors. *ACS Appl. Mater. Interfaces* **2013**, *5*, 2685−2691.
(14) Yan, J.; Fan, Z. J.; Sun, W.; Ning, G. Q.; Wei, T.; Zhang, Q.; Zhang, R. F.; Zhi, L. J.; Wei, F. Advanced Asymmetric Supercapacitors Based on $Ni(OH)_2$/Graphene and Porous Graphene Electrodes with High Energy Density. *Adv. Funct. Mater.* **2012**, *22*, 2632−2641.
(15) Bi, H.; Huang, F. Q.; Liang, J.; Tang, Y. F.; Lü, X. J.; Xie, X. M.; Jiang, M. H. Large-Scale Preparation of Highly Conductive Three Dimensional Graphene and Its Applications in CdTe Solar Cells. *J. Mater. Chem.* **2011**, *21*, 17366−17370.
(16) Kim, Y. K.; Na, H. K.; Kwack, S. J.; Ryoo, S. R.; Lee, Y.; Hong, S.; Hong, S.; Jeong, Y.; Min, D. H. Synergistic Effect of Graphene Oxide/MWCNT Films in Laser Desorption/Ionization Mass Spectrometry of Small Molecules and Tissue Imaging. *ACS Nano* **2011**, *5*, 4550−4561.
(17) Liu, R. J.; Li, S. W.; Yu, X. L.; Zhang, G. J.; Zhang, S. J.; Yao, J. N.; Keita, B.; Nadjo, L.; Zhi, L. J. Facile Synthesis of Au-Nanoparticle/Polyoxometalate/Graphene Tricomponent Nanohybrids: An Enzyme-Free Electrochemical Biosensor for Hydrogen Peroxide. *Small* **2012**, *8*, 1398−1406.
(18) Li, X. Y.; Wang, X.; Song, S. Y.; Liu, D. P.; Zhang, H. J. Selectively Deposited Noble Metal Nanoparticles on Fe_3O_4/Graphene Composites: Stable, Recyclable, and Magnetically Separable Catalysts. *Chem.—Eur. J.* **2012**, *18*, 7601−7607.
(19) Kim, M. I.; Kim, M. S.; Woo, M. A.; Ye, Y. J.; Kang, K. S.; Lee, J.; Park, H. G. Highly Efficient Colorimetric Detection of Target Cancer Cells Utilizing Superior Catalytic Activity of Graphene Oxide−Magnetic-Platinum Nanohybrids. *Nanoscale* **2014**, *6*, 1529−1536.
(20) Ye, S. B.; Feng, J. C.; Wu, P. Y. Deposition of Three-Dimensional Graphene Aerogel on Nickel Foam as a Binder-Free Supercapacitor Electrode. *ACS Appl. Mater. Interfaces* **2013**, *5*, 7122−7129.
(21) Dong, X. C.; Li, B.; Wei, A.; Cao, X. H.; Chan-Park, M. B.; Zhang, H.; Li, L. J.; Huang, W.; Chen, P. One-Step Growth of Graphene-Carbon Nanotube Hybrid Materials by Chemical Vapor Deposition. *Carbon* **2011**, *49*, 2944−2949.
(22) Wang, J. L.; Shi, Z. X.; Fan, J. C.; Ge, Y.; Yin, J.; Hu, G. X. Self-Assembly of Graphene into Three-Dimensional Structures Promoted by Natural Phenolic Acids. *J. Mater. Chem.* **2012**, *22*, 22459−22466.
(23) Chen, W. F.; Yan, L. F. In Situ Self-Assembly of Mild Chemical Reduction Graphene for Three-Dimensional Architectures. *Nanoscale* **2011**, *3*, 3132−3137.
(24) Zhou, G. W.; Wang, J. L.; Gao, P. F.; Yang, X. W.; He, Y. S.; Liao, X. Z.; Yang, J.; Ma, Z. F. Facile Spray Drying Route for the Three-Dimensional Graphene-Encapsulated Fe_2O_3 Nanoparticles for Lithium Ion Battery Anodes. *Ind. Eng. Chem. Res.* **2013**, *52*, 1197−1204.
(25) Xu, Y. X.; Sheng, K. X.; Li, C.; Shi, G. Q. Self-Assembled Graphene Hydrogel via a One-Step Hydrothermal Process. *ACS Nano* **2010**, *4*, 4324−4330.
(26) Zhang, L. N.; Deng, H. H.; Lin, F. L.; Xu, X. W.; Weng, S. H.; Liu, A. L.; Lin, X. H.; Xia, X. H.; Chen, W. In Situ Growth of Porous Platinum Nanoparticles on Graphene Oxide for Colorimetric Detection of Cancer Cells. *Anal. Chem.* **2014**, *86*, 2711−2718.
(27) Wang, C.; Daimon, H.; Sun, S. H. Dumbbell-Like Pt-Fe_3O_4 Nanoparticles and Their Enhanced Catalysis for Oxygen Reduction Reaction. *Nano Lett.* **2009**, *9*, 1493−1496.
(28) Ma, J. J.; Wang, J. L.; He, Y. S.; Liao, X. Z.; Chen, J.; Wang, J. Z.; Yuan, T.; Ma, Z. F. A Solvothermal Strategy: One-Step In Situ Synthesis of Self-Assembled 3D Graphene-Based Composites with Enhanced Lithium Storage Capacity. *J. Mater. Chem. A* **2014**, *2*, 9200−9207.
(29) Zhong, C.; Wang, J. Z.; Gao, X. W.; Wexler, D.; Liu, H. K. In Situ One-Step Synthesis of a 3D Nanostructured Germanium-Graphene Composite and Its Application in Lithium-Ion Batteries. *J. Mater. Chem. A* **2013**, *1*, 10798−10804.
(30) Zhang, Z. Y.; Sun, T.; Chen, C.; Xiao, F.; Gong, Z.; Wang, S. Bifunctional Nanocatalyst Based on Three Dimensional Carbon Nanotube-Graphene Hydrogel Supported Pd Nanoparticles: One-Pot Synthesis and Its Catalytic Properties. *ACS Appl. Mater. Interfaces* **2014**, *6*, 21035−21040.
(31) Marcano, D. C.; Kosynkin, D. V.; Berlin, J. M.; Sinitskii, A.; Sun, Z. Z.; Slesarev, A.; Alemany, L. B.; Lu, W.; Tour, J. M. Improved Synthesis of Graphene Oxide. *ACS Nano* **2010**, *4*, 4806−4814.
(32) Chen, X. M.; Wu, G. H.; Chen, J. M.; Chen, X.; Xie, Z. X.; Wang, X. R. Synthesis of "Clean" and Well-Dispersive Pd Nanoparticles with Excellent Electrocatalytic Property on Graphene Oxide. *J. Am. Chem. Soc.* **2011**, *133*, 3693−3695.
(33) Hu, J.; Dong, Y. L.; Chen, X. J.; Zhang, H. J.; Zheng, J. M.; Wang, Q.; Chen, X. G. A Highly Efficient Catalyst: In Situ Growth of Au Nanoparticles on Graphene Oxide-Fe_3O_4 Nanocomposite Support. *Chem. Eng. J.* **2014**, *236*, 1−8.
(34) Scheuermann, G. M.; Rumi, L.; Steurer, P.; Bannwarth, W.; Mülhaupt, R. Palladium Nanoparticles on Graphite Oxide and Its Functionalized Graphene Derivatives as Highly Active Catalysts for the Suzuki−Miyaura Coupling Reaction. *J. Am. Chem. Soc.* **2009**, *131*, 8262−8270.
(35) Huang, H. J.; Wang, X. Design and Synthesis of Pd-MnO_2 Nanolamella-Graphene Composite as a High-Performance Multifunctional Electrocatalyst towards Formic Acid and Methanol Oxidation. *Phys. Chem. Chem. Phys.* **2013**, *15*, 10367−10375.
(36) Li, X. Y.; Si, Z. J.; Lei, Y. Q.; Li, X. N.; Tang, J. K.; Song, S. Y.; Zhang, H. J. Hierarchically Structured Fe_3O_4 Microspheres: Morphology Control and Their Application in Wastewater Treatment. *CrystEngComm* **2011**, *13*, 642−648.
(37) Gao, H. C.; Sun, Y. M.; Zhou, J. J.; Xu, R.; Duan, H. W. Mussel-Inspired Synthesis of Polydopamine-Functionalized Graphene Hydrogel as Reusable Adsorbents for Water Purification. *ACS Appl. Mater. Interfaces* **2013**, *5*, 425−432.
(38) Jeong, H. K.; Jin, M. H.; An, K. H.; Lee, Y. H. Structural Stability and Variable Dielectric Constant in Poly Sodium 4-Styrensulfonate Intercalated Graphite Oxide. *J. Phys. Chem. C* **2009**, *113*, 13060−13064.
(39) Zhou, G. M.; Wang, D. W.; Li, F.; Zhang, L. L.; Li, N.; Wu, Z. S.; Wen, L.; Lu, G. Q.; Cheng, H. M. Graphene-Wrapped Fe_3O_4 Anode Material with Improved Reversible Capacity and Cyclic Stability for Lithium Ion Batteries. *Chem. Mater.* **2010**, *22*, 5306−5313.
(40) Yan, W.; He, F.; Gai, S. L.; Gao, P.; Chen, Y. J.; Yang, P. P. A Novel 3D Structured Reduced Graphene Oxide/TiO_2 Composite: Synthesis and Photocatalytic Performance. *J. Mater. Chem. A* **2014**, *2*, 3605−3612.
(41) Ban, C. M.; Wu, Z. C.; Gillaspie, D. T.; Chen, L.; Yan, Y. F.; Blackburn, J. L.; Dillon, A. C. Nanostructured Fe_3O_4/SWNT Electrode: Binder-Free and High-Rate Li-Ion Anode. *Adv. Mater.* **2010**, *22*, E145−E149.
(42) Sudeep, P. M.; Narayanan, T. N.; Ganesan, A.; Shaijumon, M. M.; Yang, H.; Ozden, S.; Patra, P. K.; Pasquali, M.; Vajtai, R.; Ganguli, S.; Roy, A. K.; Anantharaman, M. R.; Ajayan, P. M. Covalently Interconnected Three-Dimensional Graphene Oxide Solids. *ACS Nano* **2013**, *7*, 7034−7040.
(43) Worsley, M. A.; Pauzauskie, P. J.; Olson, T. Y.; Biener, J.; Satcher, J. H., Jr.; Baumann, T. F. Synthesis of Graphene Aerogel with High Electrical Conductivity. *J. Am. Chem. Soc.* **2010**, *132*, 14067−14069.
(44) Zhang, X. T.; Sui, Z. Y.; Xu, B.; Yue, S. F.; Luo, Y. J.; Zhan, W. C.; Liu, B. Mechanically Strong and Highly Conductive Graphene Aerogel and Its Use as Electrodes for Electrochemical Power Sources. *J. Mater. Chem.* **2011**, *21*, 6494−6497.
(45) Hu, C. G.; Zhai, X. Q.; Zhao, Y.; Bian, K.; Zhang, J.; Qu, L. T.; Zhang, H. M.; Luo, H. X. Small-Sized PdCu Nanocapsules on 3D Graphene for High-Performance Ethanol Oxidation. *Nanoscale* **2014**, *6*, 2768−2775.
(46) Chen, Y. J.; Cao, H. Y.; Shi, W. B.; Liu, H.; Huang, Y. M. Fe-Co Bimetallic Alloy Nanoparticles as a Highly Active Peroxidase Mimetic

DOI: 10.1021/am508540x
ACS Appl. Mater. Interfaces 2015, 7, 3480−3491

and Its Application in Biosensing. *Chem. Commun.* **2013**, *49*, 5013−5015.
(47) Ye, W. C.; Chang, Y. L.; Ma, C. L.; Jia, B. Y.; Cao, G. Y.; Wang, C. M. Electrochemical Investigation of the Surface Energy: Effect of the HF Concentration on Electroless Silver Deposition onto *p*-Si(111). *Appl. Surf. Sci.* **2007**, *253*, 3419−3424.
(48) Gao, L. Z.; Zhuang, J.; Nie, L.; Zhang, J. B.; Zhang, Y.; Gu, N.; Wang, T. H.; Feng, J.; Yang, D. L.; Perrett, S.; Yan, X. Y. Intrinsic Peroxidase-Like Activity of Ferromagnetic Nanoparticles. *Nat. Nanotechnol.* **2007**, *2*, 577−583.
(49) Ishibashi, K.; Fujishima, A.; Watanabe, T.; Hashimoto, K. Quantum Yields of Active Oxidative Species Formed on TiO_2 Photocatalyst. *J. Photochem. Photobiol., A* **2000**, *134*, 139−142.
(50) Sturgeon, B. E.; Battenburg, B. J.; Lyon, B. J.; Franzen, S. Revisiting the Peroxidase Oxidation of 2,4,6-Trihalophenols: ESR Detection of Radical Intermediates. *Chem. Res. Toxicol.* **2011**, *24*, 1862−1868.
(51) Sun, X. L.; Guo, S. J.; Liu, Y.; Sun, S. H. Dumbbell-Like PtPd-Fe_3O_4 Nanoparticles for Enhanced Electrochemical Detection of H_2O_2. *Nano Lett.* **2012**, *12*, 4859−4863.
(52) Wesner, D. A.; Johnson, P. D.; Smith, N. V. Photoemission Spectra and Band Structures of D-Band Metals. 11. Inverse Photoemission from Pd(111). *Phys. Rev. B* **1984**, *30*, 503−506.
(53) Weiss, W.; Ranke, W. Surface Chemistry and Catalysis on Well-Defined Epitaxial Iron-Oxide Layers. *Prog. Surf. Sci.* **2002**, *70*, 1−151.
(54) Lin, S. X.; Shen, C. M.; Lu, D. B.; Wang, C. M.; Gao, H. J. Synthesis of Pt Nanoparticles Anchored on Graphene-Encapsulated Fe_3O_4 Magnetic Nanospheres and Their Use as Catalysts for Methanol Oxidation. *Carbon* **2013**, *53*, 112−119.
(55) Solozhenko, E. G.; Soboleva, N. M.; Goncharuk, V. V. Decolourization of Azodye Solutions by Fentons Oxidation. *Water Res.* **1995**, *29*, 2206−2210.
(56) Liu, Y. P.; Yu, F. Q. Substrate-Specific Modifications on Magnetic Iron Oxide Nanoparticles as an Artificial Peroxidase for Improving Sensitivity in Glucose Detection. *Nanotechnology* **2011**, *22*, 145704.
(57) Fromm, H. J.; Hargrove, M. In *Essentials of Biochemistry*; Springer−Verlag: Berlin, Heidelberg, Germany, 2012; Chapter 5, pp 108−109.
(58) Garrett, R. H.; Grisham, C. M. In *Biochemistry*; Cengage Learning: Belmont, CA, 2010; Chapter 13, pp 406−407.
(59) Su, L.; Feng, J.; Zhou, X. M.; Ren, C. L.; Li, H. H.; Chen, X. G. Colorimetric Detection of Urine Glucose Based $ZnFe_2O_4$ Magnetic Nanoparticles. *Anal. Chem.* **2012**, *84*, 5753−5758.
(60) Pachla, L. A.; Reynolds, D. L.; Wright, D. S.; Kissinger, P. T. Analytical Methods for Measuring Uric Acid in Biological Samples and Food-Products. *J.−Assoc. Off. Anal. Chem.* **1987**, *70*, 1−14.
(61) Urakami, T.; Suzuki, J.; Yoshida, A.; Saito, H.; Mugishima, H. Incidence of Children with Slowly Progressive Form of Type 1 Diabetes Detected by the Urine Glucose Screening at Schools in the Tokyo Metropolitan Area. *Diabetes Res. Clin. Pract.* **2008**, *80*, 473−476.

DOI: 10.1021/am508540x
ACS Appl. Mater. Interfaces 2015, 7, 3480−3491